ISSN 0022-4766, Journal of Structural Chemistry, 2024, Vol. 65, No. 1, pp. 1-14. © Pleiades Publishing, Ltd., 2024.
Text © The Author(s), 2024, published in Zhurnal Strukturnoi Khimii, 2024, Vol. 65, No. 1, 119220.

STRUCTURAL ELUCIDATION, HIRSHFELD SURFACE, FMO, MOLECULAR ELECTROSTATIC POTENTIAL (MEP) AND FUKUI FUNCTION ANALYSES OF A QUINOLINE BASED SCHIFF BASE COMPOUND

S. Halder[1], P. C. Mandal[2], M. Guin[3]*, and S. Konar[4]**

A quinoline-derived Schiff base ligand, namely 2,5-Dimethyl-N1,N4-bis((quinoline-4-yl)-methylene) benzene-1,4-diamine **1** was characterized by single crystal X-ray structural studies that included a thorough examination of visualizing and investigating intermolecular interactions in molecular crystals *via* the Hirshfeld surface. The crystal packing of **1** displays intermolecular π···π stacking interactions, resulting in a one-dimensional array. The major role of π···π stacking interactions in stabilizing the crystal is also supported by the pre-eminence of dispersion energy over the other components in interaction energy calculation and energy framework analysis. The electronic structure of the ligand computed at B3LYP/6-311++G(*d*,*p*) level shows a good correlation with the experimentally obtained structure. Additionally, the Fukui function is calculated to identify the electrophilic and nucleophilic active sites in the molecule.

DOI: 10.1134/S0022476624010013

Keywords: crystal structure, DFT, Hirshfeld surface.

INTRODUCTION

Supramolecular chemistry as well as the related disciplines that use molecular recognition rely considerably on a detailed understanding of the recognition properties of the functional groups engaged in noncovalent interactions. Noncovalent interactions have recently received a lot of interest in the domains of chemistry, biology, and materials science. π···π interactions are prominent among the several noncovalent interactions that exist between molecules in aromatic systems. One of the most contentious supramolecular interactions is π···π interaction, which has been studied from the inception of the discipline of crystal engineering [1-5]. The number of research articles on this topic is growing along with the number of research organisations in the area of crystal engineering. Publications on this subject have increased during the last two decades and continue to do so.

Additionally, comprehending numerous non-covalent interactions like electrostatic force, hydrogen bonding, π···π stacking, and Van der Waals interactions is greatly aided by DFT calculations. These interactions act as prime forces in

[1]Department of Chemistry, T.N.B. College, Bhagalpur, Bihar, Republic of India. [2]Department of Chemistry, Raja Rammohun Roy Mahavidyalaya, Hooghly, Republic of India. [3]Department of Chemistry and Biochemistry, Sharda University, Greater Noida, Uttar Pradesh, Republic of India; *mridula.guin@sharda.ac.in. [4]Department of Chemistry, The Bhawanipur Education Society College, Kolkata, Republic of India; **saugata.konar@gmail.com. Original article submitted July 1, 2023; revised August 14, 2023; accepted September 6, 2023.

building supramolecular assembly [6, 7]. Accurate prediction of molecular geometry, intermolecular interaction energy, and stability of the supramolecular system can be done using DFT calculations. The supramolecular motifs in a molecular structure can be visualized through Hirshfeld surface analysis, fingerprint plots and 3D energy framework analysis. In the present work the electronic structure, molecular electrostatic potential (MEP), and frontier molecular orbital (FMO) analysis has been carried out using DFT calculations. Along with this, Hirshfeld surface analysis is performed to understand intermolecular interactions and surface properties of the molecular crystal.

Herein, we report the characteristics of the quinoline-based ligand skeleton and its molecular structure and to investigate the possibilities for the inter and intramolecular π···π contacts in the solid state, the X-ray structure analysis was undertaken along with the Hirshfeld surface analysis to investigate the close contacts.

EXPERIMENTAL

Materials and measurements. All reagents and chemicals were of AR grade and obtained from commercial sources (SD Fine Chemicals, India; and Aldrich) and used without further purification.

Preparation of 2,5-Dimethyl-N1,N4-bis((quinolin-4-yl)-methylene)benzene-1,4-diamine (Me_2-BQD) (1). 2,5-Dimethyl-N1,N4-bis((quinoline-4-yl)-methylene)benzene-1,4-diamine (**1**) (Scheme 1) was prepared by simple condensation reaction between 2 mmol of Quinoline-4-carboxaldehyde and 1 mmol of 2,5-dimethyl-1,4-diaminobenzene in methanol medium [8]. Yellow block shaped crystals were obtained after recrystallization from a toluene medium (Yield: 67%).

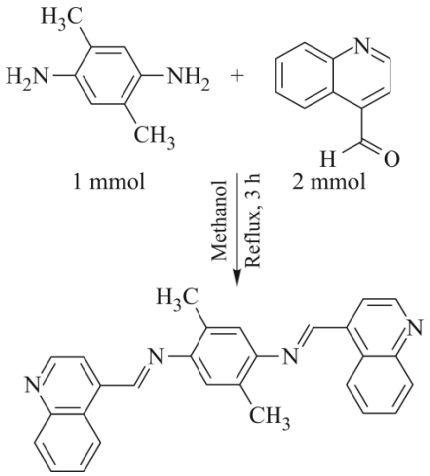

Scheme 1. Scheme of synthesis of 2,5-Dimethyl-N1,N4-bis((quinolin-4-yl)-methylene) benzene-1,4-diamine (**Me_2-BQD**).

Crystallographic data collection and refinement. An appropriate yellow coloured single crystal of **1** was mounted on the tip of a glass fiber coated with commercially available super glue. X-ray single crystal data were collected at room temperature using a Bruker APEX II diffractometer, equipped with a fine-focus, sealed tube X-ray source with graphite monochromated MoK_α radiation (λ = 0.71073 Å). The data were integrated using a SAINT program [9] and absorption correction was made with SADABS. The structure was solved with the help of SHELXT [10] following direct methods and refined by full-matrix least-squares on F^2 using SHELXL-2016/6 [11] with anisotropic displacement parameters for all non-hydrogen atoms. All the hydrogen atoms were fixed geometrically and placed in ideal positions. Data collection and structure refinement parameters are given in Table 1.

Density Functional Theory (DFT) study. The DFT calculations are performed using Gaussian16 program package [12]. The geometry optimization was carried out by hybrid B3LYP functional with 6-311++G** basis set. The hybrid B3LYP

TABLE 1. Crystal data for **Me2-BQD** (**1**)

Parameter	Data
Formula	$C_{28}H_{22}N_4$
Formula weight	414.49
Crystal system	Monoclinic
Space group	*P*21/*c*
a, *b*, *c*, Å	7.6728(17), 4.0013(9), 33.579(9)
β, deg	90.055(18)
V, Å^3	1030.9(4)
Z	2
D_c, g/cm^3	1.335
M, mm^{-1}	0.08
F(000)	436
θ range, deg	1.21-27.86
Collected/ unique/ Reflections $I > 2\sigma(I)$	14262/2350/900
R_{int}	0.2008
Goodness-of-fit (F^2)	1.011
R_1 ($I > 2\sigma(I)$)[#1]	0.0839
wR_2[#2]	0.1950
$\Delta\rho_{max/min}$, e/Å^3	–0.27, 0.32

[#1] $R_1 = \Sigma||F_o| - |F_c||/\Sigma|F_o|$;

[#2] $wR^2 = [\Sigma(w(F_o^2 - F_c^2)^2) / \Sigma w(F_o^2)^2]^{1/2}$.

functional is well known for predicting accurate geometrical parameters with limited computational cost. The convergence criteria were maintained at default level without any constraint on the geometry. The visualization of the electronic structure was performed using Gaussview 6.0 program. The absence of negative frequency confirms the optimized geometry of the molecule as true minima on the potential energy surface. The energy of HOMO (Highest Occupied Molecular Orbital), LUMO (Lowest Unoccupied Molecular Orbital) and band gap is determined to understand the chemical reactivity of the compound. Moreover, the molecular electrostatic potential of the compound is calculated from the electron density to predict the electrophilic and nucleophilic regions in the molecule. Additionally, the Fukui function is calculated to identify the active sites for electrophilic and nucleophilic attacks in the molecule.

Molecular Hirshfeld surface analysis. Hirshfeld surface analysis is a widely used tool for understanding the intermolecular interactions in a molecular crystal [13]. The intermolecular close contacts can be visualized both qualitatively and quantitatively through the Hirshfeld surface. The red-white-blue colour surface of the normalized contact distance d_{norm} identifies the close contacts around Van der Waals radius, short contacts and long contacts. The mapped d_{norm} surface shows red spots wherever close contacts are present in the molecular crystal.

Crystal Explorer 17.5 program [14] is used to perform Hirshfeld surface (HS) analysis of the complex. The Hirshfeld surface was generated using a high standard surface resolution. Three colour-coded surfaces e.g., d_{norm}, shape index and curvedness were mapped for the molecular crystal. All the surfaces were presented in a transparent mode for clear visualization. Additionally, 2D fingerprint plots in terms of d_e and d_i are determined to summarize the nature and type of intermolecular contacts used in the packing of the molecular crystal.

The interaction energies between clusters of molecules within the radius of 3.8 Å around the central molecule are calculated at CE-B3LYP/6-31G(*d*,*p*) level of theory. The total energy of the molecular cluster is decomposed into electrostatic energy, exchange repulsion energy, polarization energy and dispersion energy. The energy frameworks were constructed to visualize the topology of the computed interaction energies.

RESULTS AND DISCUSSION

Description of the crystal structure. The synthesis of 2,5-Dimethyl-N1,N4-bis((quinoline-4-yl)-methylene) benzene-1,4-diamine has been performed by simple condensation reaction between 1equivalent of 2,5-dimethyl-1,4-diaminobenzene and 2 equivalent of quinoline-4-carboxaldehyde in methanol medium. Recrystallization from toluene produced single crystals of the compound suitable for single-crystal X-ray diffraction analysis. X-ray diffraction analysis reveals that the compound crystallizes in the monoclinic *P*21/*c* space group. A thermal ellipsoid plot of **1** is presented in Fig. 1 and details bond lengths and angles are in Table 2. The asymmetric unit of the compound consists of a quinoline moiety, an imine group, along with half of a six-member dimethyl substituted aromatic ring. The crystal structure of the molecule shows that it is not at all planar. Actually, two quinoline rings within the molecule reside in the same plane and

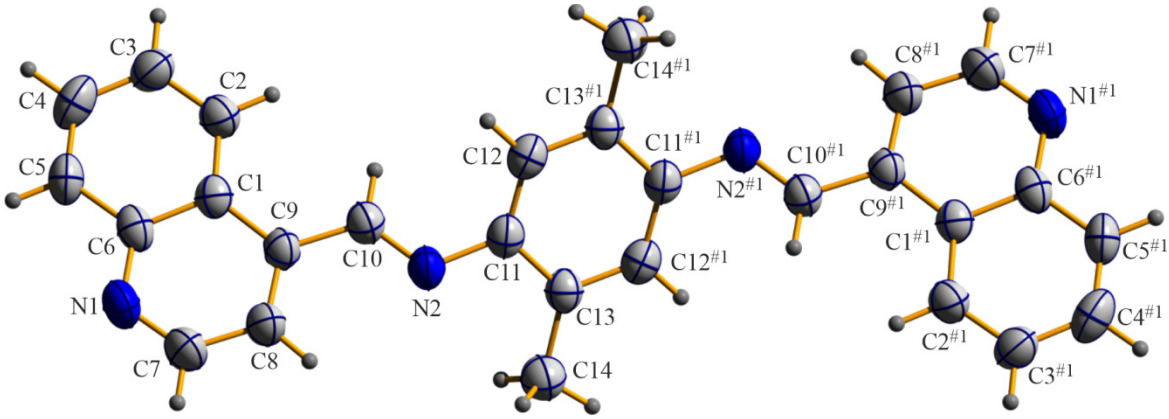

Fig. 1. ORTEP diagram (50% ellipsoid probability) of **1**. Symmetry code[#1]: 2−*x*, 1−*y*, −*z*.

TABLE 2. Comparison of the Structural Analysis with the Literature Value

Compound	Color	*V* (C=N), cm^{-1}	Recrystallization from solvent	^{1}H NMR (imine), ppm	Yield, %	λ, nm	Mass spectra (*m*/*z*)	Ref.
(Me_2-BQD)	Yellow	1601	Toluene	9.09	74	325, 465	4134.19	Our work
SL_1	Whitish-yellow	1500	Hot ethanol	8.58-8.98	82	295, 324	320.22	[15]
SL_2	Off-white	1502	Hot ethanol		89	284, 326	350.19	
SL_3	Yellow	1504	Hot ethanol		94	262, 322	369.39	
SL_4	Yellowish-white	1505	Hot ethanol		78	301, 317	304.31	
2a	Yellow	1609	Ethanol	9.94	68.5	–	395	[16]
2b	Yellow	1615	Ethanol	9.31	59.3	–	388	
2c	Yellow	1613	Acetic acid	9.87	55.4	–	434.7	
DBQA	–	1610	Ethanol	9.13	75	237, 312	–	[17]
VII	Yellow	1616	DMSO	7.99	74		382	[18]
HL	Light yellow	1615	DMSO	9.42	75	–	358	[19]
BQB	Light yellow	–	Toluene	8.7	70	380, 402	387.01	[20]

the central aromatic ring is residing in a dissimilar plane from that of the two quinoline moieties. The torsion angle is observed as 41.16°. It has been observed that there are three types of π···π interactions (Fig. 2). Firstly, the pyridine ring moiety, *Cg*1 (*Cg*1 = N1–C6–C1–C9–C8–C7) with a pyridine ring *Cg*1 (*Cg*1 = N1–C6–C1–C9–C8–C7) of second unit, secondly, aromatic benzene ring, *Cg*2 (*Cg*2 = C1–C2–C3–C4–C5–C6) with benzene ring *Cg*2 (*Cg*2 = C1–C2–C3–C4–C5–C6) of second unit and third, aromatic benzene ring, *Cg*3 (*Cg*3 = C11–C12–C13a–C11a–C12a–C13) with benzene ring *Cg*2 (*Cg*3 = C11–C12–C13a–C11a–C12a–C13) of second unit leads to the formation of a 1D unit in **1**. A comparative study between our quinoline based Schiff base compound **Me_2-BQD** (**1**) and several other quinoline based organic compounds are presented in Table 2.

Geometry. The energy minimized structure of the molecule is shown in Fig. 3. The structural parameters along with the crystallographic data of the molecule are listed in Table 3. The computed bond distance and angles are in good agreement with the experimental geometrical parameters.

Frontier Molecular Orbital (FMO) analysis. The frontier molecular orbital analysis was performed to determine the global reactivity descriptors. The energy gap between frontier molecular orbitals (HOMO and LUMO) of a molecule is an important parameter to predict the stability and reactivity of the system. Various quantum chemical descriptors such as ionization potential (*I*) and electron affinity (*A*), global hardness (η), global softness (*S*), electronegativity (χ), chemical potential (μ) and electrophilicity index (ω) of the molecule is computed and summarized in Table 4. The computed surface plots of HOMO and LUMO are displayed in Fig. 4. The low band gap (3.211 eV) predicts the molecule to be chemically

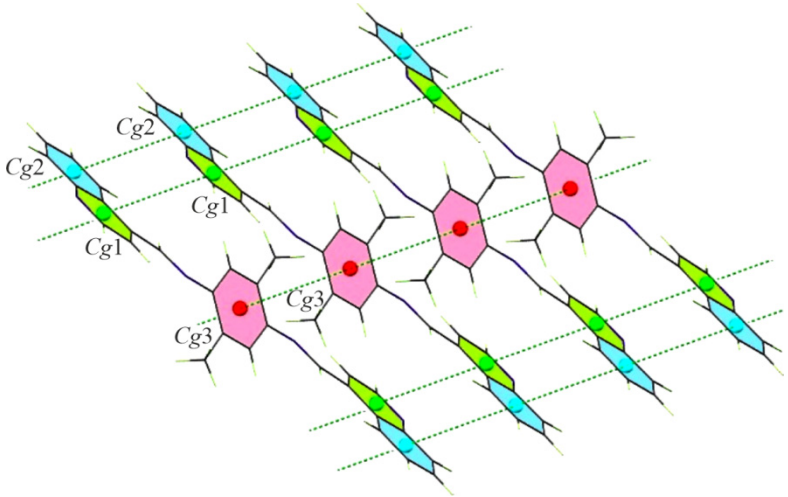

Fig. 2. Strong π···π interactions observed in **1** to form 1D architecture**.**

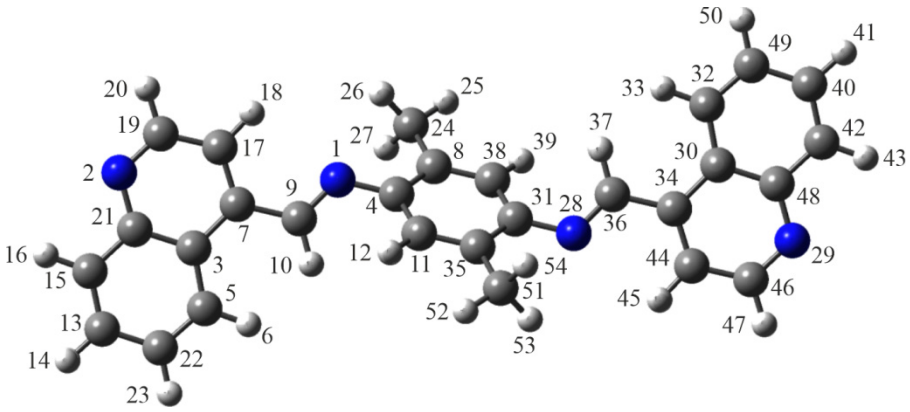

Fig. 3. DFT/B3-LYP/6–311++G(*d*,*p*) optimized structure of the molecule.

TABLE 3. Selected Bond Lengths and Bond Angles

Bond	Length, Å		Angle	Value, deg	
	XRD	DFT		XRD	DFT
1	2	3	4	5	6
N1–C9	1.270(5)	1.278	C9–N1–C4	117.7(4)	120.65
N1–C4	1.422(5)	1.403	C19–N2–C21	116.4(3)	117.76
N2–C19	1.306(5)	1.316	C5–C3–C21	118.0 (4)	118.08
N2–C21	1.371(5)	1.362	C5–C3–C7	125.0(3)	124.69
C3–C5	1.408(5)	1.421	C21–C3–C7	117.0(4)	117.22
C3–C21	1.415(5)	1.434	C11–C4–C8	120.0(3)	119.64
C3–C7	1.430(5)	1.433	C11–C4–N1	122.9(3)	122.18
C4–C11	1.382(6)	1.404	C8–C4–N1	117.0(4)	118.12
C4–C8	1.402(5)	1.411	C22–C5–C3	121.8(4)	120.97
C5–C22	1.355(5)	1.375	C22–C5–H6	119.1	118.81
C5–H6	0.9500	1.082	C3–C5–H6	119.1	120.21
C7–C17	1.364(5)	1.382	C17–C7–C3	117.7(3)	118.01
C7–C9	1.462(5)	1.472	C17–C7–C9	120.9(4)	120.11
C8–C38	1.372(5)	1.391	C3–C7–C9	121.4(4)	121.87
C8–C24	1.496(6)	1.507	C38–C8–C4	117.6(4)	117.91
C36–H37	0.9500	1.093	C38–C8–C24	120.7(3)	121.14
C38–H39	0.9500	1.084	C4–C8–C24	121.7(4)	120.89
C13–C15	1.351(6)	1.372	N1–C9–C7	122.1(4)	121.86
C13–C22	1.395(6)	1.413	N1–C9–H10	119.0	120.74
C13–H14	0.9500	1.084	C7–C9–H10	119.0	117.39
C15–C21	1.412(5)	1.419	C35–C11–C4	118.8	122.42
C15–H16	0.9500	1.083	C35–C11–H12	118.8	118.77
C17–C19	1.394(5)	1.407	C15–C13–C22	121.1(4)	120.04
C17–H18	0.9500	1.082	C15–C13–H14	119.4	120.25
C19–H20	0.9500	1.087	C22–C13–H14	119.4	119.70
C22–H23	0.9500	1.084	C13–C15–C21	120.4(4)	120.74
C24–H25	0.9800	1.091	C13–C15–H16	119.8	121.93
C24–H27	0.9800	1.094	C21–C15–H16	119.8	117.32
C24–H26	0.9800	1.092	C7–C17–C19	120.6(4)	119.89
			C7–C17–H18	119.7	119.51
			C19– C17–H18	119.7	120.59
			N2–C19–C17	124.5(4)	124.06
			N2–C19–H20	117.8	116.35
			C17–C19–H20	117.8	119.57
			N2–C21–C15	117.1(4)	117.49
			N2–C21–C3	123.7(4)	123.03
			C15–C21–C3	119.1(4)	119.47
			C5–C22–C13	119.6(4)	120.68
			C5–C22–H23	120.2	119.68
			C13–C22–H23	120.2	119.63
			C8–C24–H25	109.5	110.90
			C8–C24–H27	109.5	111.41
			H25–C24–H27	109.5	107.95

TABLE 3. (Cont.)

1	2	3	4	5	6
			C8–C24–H26	109.5	110.8
			H25–C24–H26	109.5	108.96
			H27–C24–H26	109.5	106.62

TABLE 4. FMO Energy Parameters and Global Reactivity Descriptors of the Molecule

Parameter, eV	Value
HOMO	6.013
LUMO	–2.802
ΔE = (LUMO–HOMO)	3.211
$I = -E$(HOMO)	6.013
$A = -E$(LUMO)	2.802
$\chi = (I + A)/2$	4.407
$M = -\chi$	–4.407
$\eta = (I - A)/2$	1.605
$S = 1/\eta$	0.623
$\Omega = \mu^2/2\,\eta$	6.048

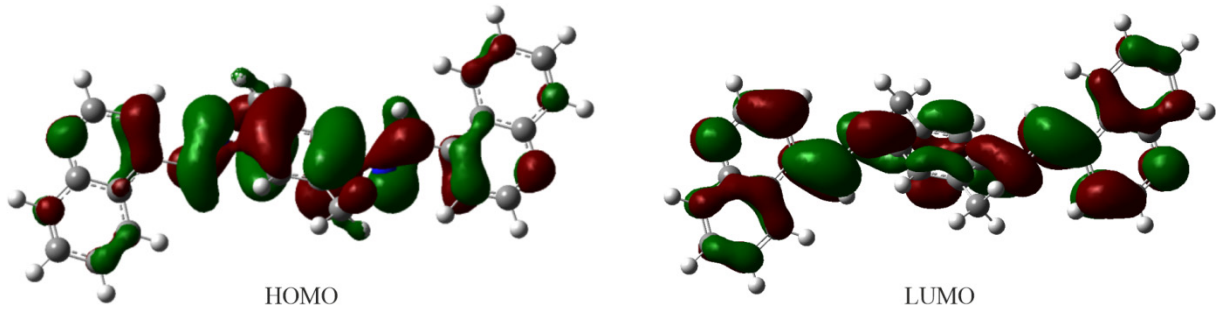

Fig. 4. 3D surface plots of HOMO and LUMO of the molecule.

reactive through the facile charge transfer process. Further, the small hardness value (1.605 eV) of the molecule signifies easy alteration of the electron density and predicts high reactivity of the molecule.

Local reactivity descriptors. The Fukui function is considered one of the important reactivity descriptors. It is based on the concept of the change in the number of electrons under a constant external potential in a molecule that changes the electron density function of the molecule [21, 22]. The Fukui function identifies the most reactive sites in terms of electrophilic and nucleophilic reactions within the molecule. A chemical reaction involves the addition or subtraction of electrons in the frontier orbitals. The propensity of deformation of electron density at a particular position due to a change in the number of electrons is predicted by the condensed Fukui function. Various types of Fukui functions for j_{th} atom are defined as follows:

$$f_+ = [q(N + 1) - q(N)]; \text{ Nucleophilic site,}$$
$$f_- = [q(N) - q(N - 1)]; \text{ Electrophilic site,}$$
$$f_0 = [q(N + 1) - q(N - 1)]/2; \text{ Radical site,}$$

q(N) signifies the electronic charge on the jth atom for the neutral molecule, q(N + 1) is the charge for the anionic molecule and q(N – 1) is the same for the cationic species. These descriptors are presented in Table 5 that are calculated using B3LYP/6-311++G(d,p) level using NBO charges on the respective atoms.

TABLE 5. Fukui Function Values of the Molecule

Atom	f_+	f_-	f_0
N1	–0.049	–0.017	–0.033
N2	–0.072	–0.058	–0.065
C3	–0.004	–0.005	–0.0045
C4	–0.03	–0.055	–0.0425
C5	–0.003	–0.014	–0.0085
H6	–0.003	0.001	–0.001
C7	–0.019	0.008	–0.0055
C8	**0.023**	–0.088	–0.0325
C9	–0.062	–0.05	–0.056
H10	–0.014	–0.014	–0.014
C11	0.013	–0.031	–0.009
H12	–0.009	–0.017	–0.013
C13	–0.023	–0.015	–0.019
H14	–0.015	–0.015	–0.015
C15	–0.023	–0.032	–0.0275
H16	–0.013	–0.013	–0.013
C17	–0.049	–0.038	–0.0435
H18	–0.008	–0.002	–0.005
C19	–0.012	0.002	–0.005
H20	–0.018	–0.015	–0.0165
C21	–0.001	0.003	0.001
C22	–0.03	–0.029	–0.0295
H23	–0.014	–0.012	–0.013
C24	0	**0.015**	**0.0075**
H25	–0.011	–0.016	–0.0135
H26	–0.005	–0.013	–0.009
H27	–0.009	–0.019	–0.014
C31	0.014	–0.098	–0.042
C35	–0.052	–0.013	–0.0325
C38	–0.047	0.029	–0.009
H39	–0.007	–0.018	–0.0125
C51	0.009	0.006	**0.0075**
H52	–0.011	–0.016	–0.0135
H53	–0.005	–0.013	–0.009
H54	–0.009	–0.019	–0.014

The data indicates the most preferable nucleophilic site of the molecule is located on the C8 atom while the most reactive electrophilic site is C24. The most susceptible site for free radical attack in the molecule is C24 or C51 atom.

Molecular Electrostatic Potential (MEP). The electrostatic potential of a molecular entity is a valuable tool to predict electrophilic and nucleophilic sites within the molecule. The propensity of formation of various types of intermolecular interactions for example, hydrogen bonding, drug-receptor interaction, enzyme-substrate interactions etc is

majorly based on the electrostatic potential of the molecule. The MEP of the molecule is calculated using the electron density of the optimized structure at B3LYP/6-311++G(*d*,*p*) level and displayed in Fig. 5. The figure indicates the presence of high electron density or negative charge around the nitrogen atoms of the pyridine rings (red colored surface) while the methyl groups present at the para positions of the benzene ring is electron deficient (yellow to green colored surface). Thus, the nucleophilic reactivity of the complex will be centered around the methyl groups and electrophilic reactivity around the pyridine rings of the molecule.

Hirshfeld surface analysis. The Hirshfeld surfaces of the compound mapped in terms of d_{norm}, curvedness and shape index are shown in Fig. 6. The d_{norm} surface represents the normalized contact distance. The two red spots in the d_{norm} surface indicate the atoms present in close proximity to the outer side of the Hirshfeld surface arising due to the C–H···H–C interactions. The white and blue surfaces indicate atoms with medium proximity and large distance respectively from the Hirshfeld surface. The shape index and curvedness determine the shape and surface area of the molecule. The shape index is a key parameter in understanding the presence of π···π stacking interactions in the packing modes of the crystal. A few adjacent red and blue triangles in the shape index of the molecule imply the presence of weak π···π stacking interactions. The red triangles in the concave region are above the surface plane and are stacked over the blue triangles inside the surface plane in the concave region. Further, the curvedness map supports the findings of the shape index. The presence of flat surface patches in the curvedness map clearly tells that the crystal is packed with weak π···π stacking interactions. The intermolecular interactions in the molecule are also depicted in Fig. 6.

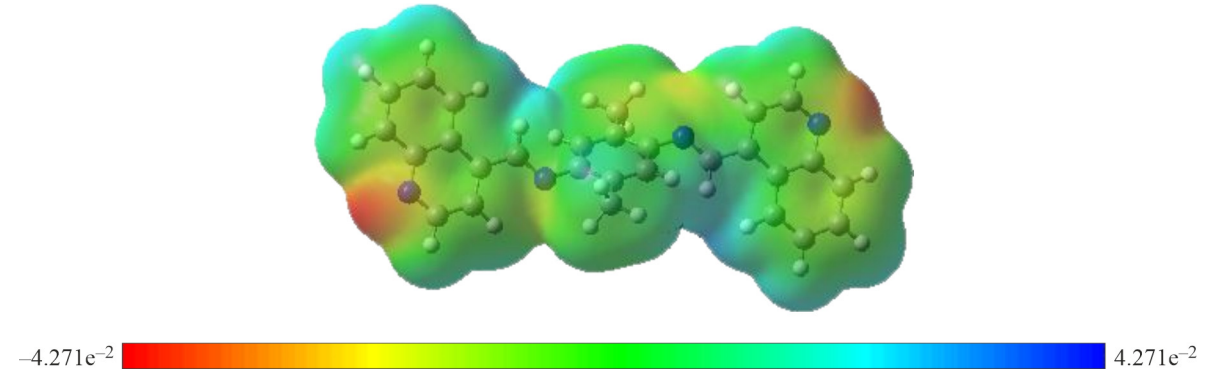

Fig. 5. Molecular electrostatic potential map of the molecule.

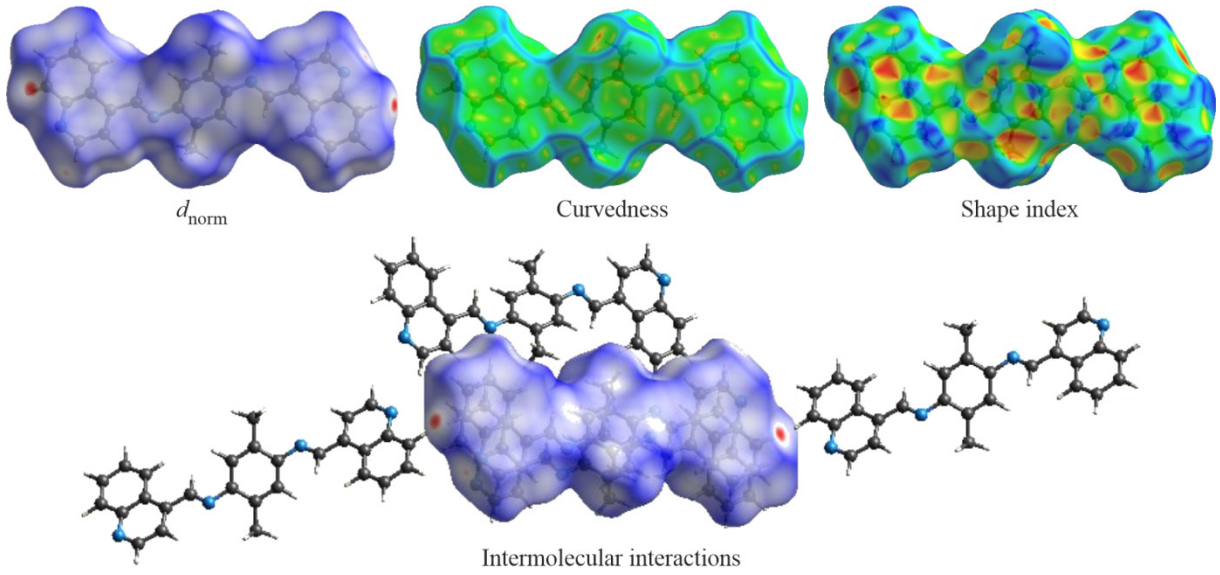

Fig. 6. Two-dimensional fingerprint plot of the molecule showing the contributions of individual interactions.

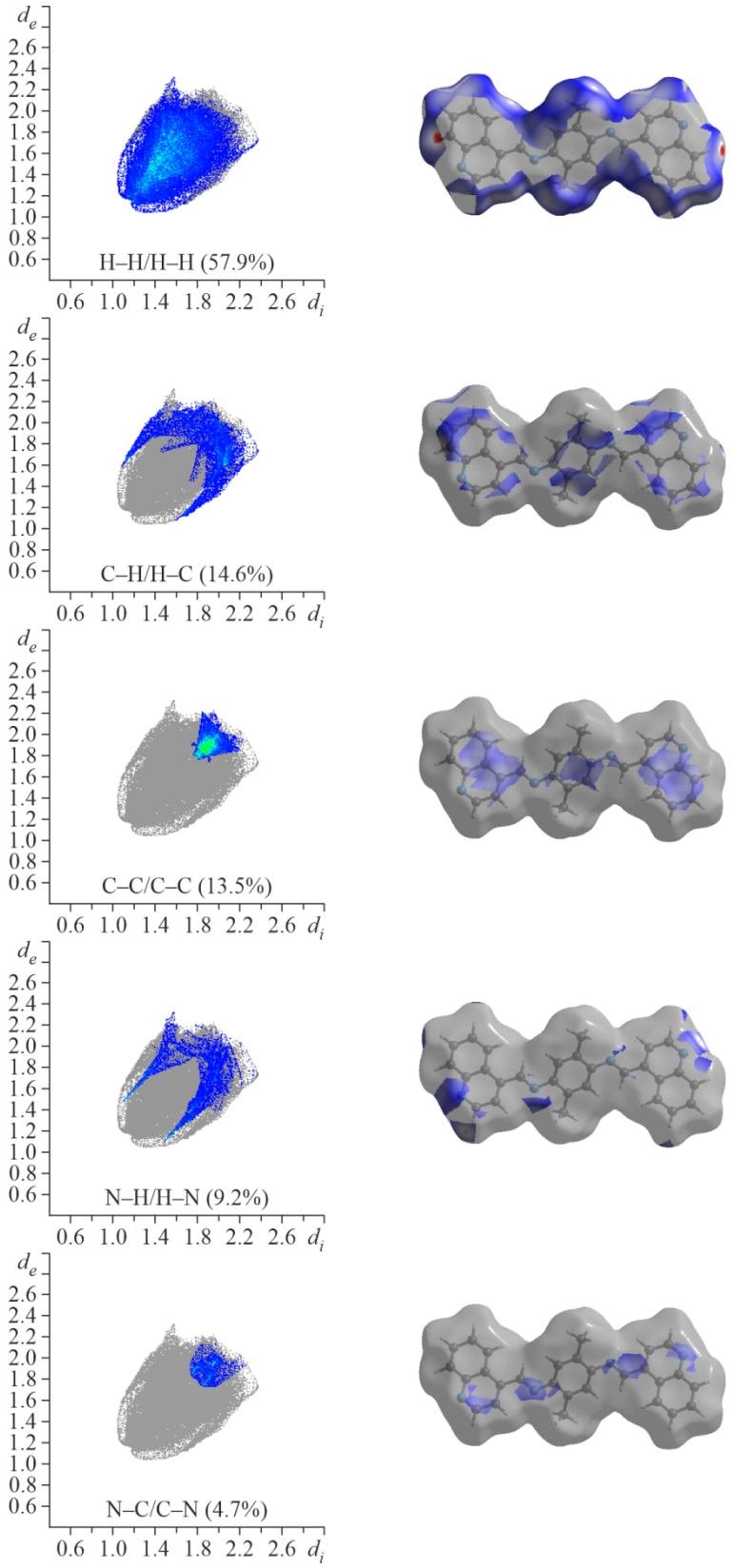

Fig. 7. Two-dimensional fingerprint plot of the molecule showing the contributions of individual interactions. Surfaces to the right of each FP plots highlight the relevant surface patches associated with the specific contacts with d_{norm} mapped.

The two-dimensional fingerprint plots (Fig. 7) of the major contacts are determined to quantify the intermolecular interactions. The molecular crystal has H···H contacts as major interactions contributing 57.9% to the overall crystal packing. The next contribution is from C···H/H···C contacts with a 14.6% contribution in stabilizing the molecular crystal. In addition to this, other notable interactions are C···C with 13.5%, N···H (large spike) with 9.2% and N···C with 4.7% contribution in the packing of the molecular crystal. The presence of bow-tie patterns and characteristic wings in the FP plot of C···H contacts implies stabilizing effect through weak π···π stacking interactions and C–H···π interaction in the crystal [23, 24].

Interaction energy and energy framework analysis. The interaction energy between different molecular pairs in the crystal is resolved into Coulomb energy, dispersion energy and total energy which are depicted graphically in Fig. 8 along the *b* axis. The resolved energy components are described in Table 6. The properties of the crystal are directly linked to these

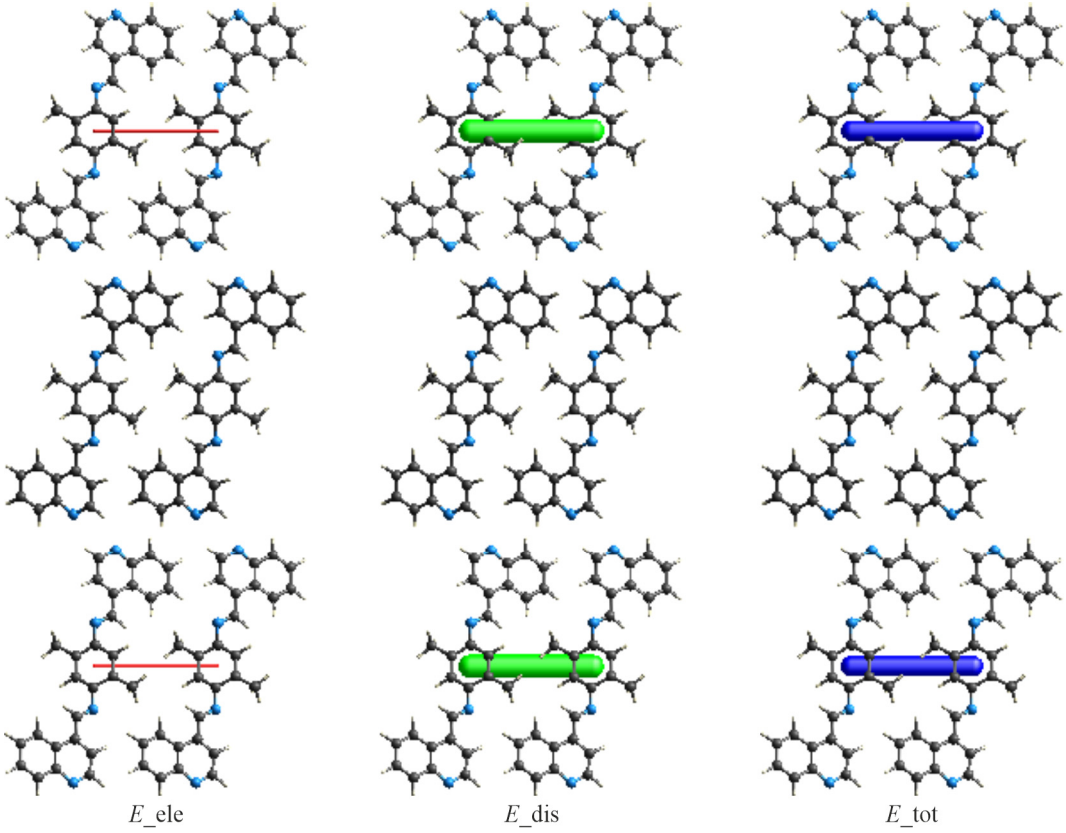

Fig. 8. Energy framework corresponding to the different energy components viewed along the *b* axis of the molecule.

TABLE 6. Interaction Energy (kJ/mol) of the Compound

N	Symmetry operation	*R*	Electron Density	*E*_ele	*E*_pol	*E*_dis	*E*_rep	*E*_tot
1	*x, y, z*	7.67	B3LYP/6-31G(*d,p*)	–5.7	–1.0	–41.5	18.1	–31.7
1	*x, y, z*	8.65	B3LYP/6-31G(*d,p*)	–7.1	–1.5	–37.3	27.7	–24.0
2	–*x*, *y*+1/2, –*z*+1/2	16.91	B3LYP/6-31G(*d,p*)	–1.9	–1.7	–7.9	0.0	–10.2
2	*x, y, z*	4.00	B3LYP/6-31G(*d,p*)	–6.0	–3.1	–139.1	64.5	–89.9
1	*x, y, z*	8.65	B3LYP/6-31G(*d,p*)	–0.2	–0.2	–7.7	1.8	–5.9
2	–*x*, *y*+1/2, –*z*+1/2	18.57	B3LYP/6-31G(*d,p*)	1.9	–0.9	–12.3	0.0	–9.4

energies. The energy diagram depicts cylinders of different thicknesses for Coulomb energy (red colour), dispersion energy (green colour) and total energy (blue colour). The thickness of the cylinders is comparable to the relative strength of the corresponding interaction energy. For the studied cluster, the total electrostatic energy is −19.0 kJ/mol, dispersion energy is −245.8 kJ/mol, polarization energy is −8.4 kJ/mol, repulsion energy is 112.1 kJ/mol and the total interaction energy is −171.1 kJ/mol. The results reveal the dispersion energy as the major component in stabilizing the molecular crystal structure.

CONCLUSIONS

In this article, we have reported the crystal structure of a quinoline-based Schiff base compound 2,5-Dimethyl-N1,N4-bis((quinoline-4-yl)-methylene)benzene-1,4-diamine. The single crystal X-ray diffraction analysis of this molecule also reveals the presence of interesting supramolecular π···π interaction within the crystal. DFT calculation at B3LYP/6-311++G(*d*,*p*) level predicts the experimental structure accurately with a minor mismatch. H···H contacts (57.9%) and C···H/H···C contacts (14.6%) are major contributors in stabilizing the molecular crystal as identified from Hirshfeld surface analysis. The C···H contacts in the FP plot display the bow-tie patterns and characteristic wings which is another confirmation of stabilizing effect through π–π stacking interactions in the crystal. Along with this the energy framework analysis also confirmed the dispersion energy as the primary force in intermolecular interaction energy calculation. The MEP plot and Fukui function calculation identifies the nucleophilic reactivity and electrophilic reactivity around the methyl groups and pyridine rings of the ligand respectively.

FUNDING

S. Konar is thankful to The Bhawanipur Education Society College, Kolkata 700020 for providing research grant (Project No. BESC/RPC/2019–2020/SC1/02).

ADDITIONAL INFORMATION

CCDC 2260461 contains the supplementary crystallographic data for **1**. These data can be obtained free of charge *via* http://www.ccdc.cam.ac.uk/conts/retrieving.html, or from the Cambridge Crystallographic Data Centre, 12 Union Road, Cambridge CB2 1EZ, UK; fax: (+44) 1223-336-033; or e-mail: deposit@ccdc.cam.ac.uk.

CONFLICT OF INTERESTS

The authors of this work declare that they have no conflicts of interest.

REFERENCES

1. G. R. Desiraju and A. Gavezzotti. Crystal structures of polynuclear aromatic hydrocarbons. Classification, rationalization and prediction from molecular structure. *Acta Crystallogr*., *Sect*. *B: Struct*. *Sci*., **1989**, *45*, 473-482. https://doi.org/10.1107/S0108768189003794
2. Y. Liu, Y.-H. Zhou, X.-L. Liao, L.-M. Man, B.-W. Wang, J.-R. Zhou, and C.-L. Ni. Crystal structure and magnetic properties of a hybrid compound: Disubstituted benzyl dimethylaminopyridinium bis(maleonitriledithiolate)cuprate(II). *J*. *Struct*. *Chem*., **2017**, *58*(8), 1656-1662. https://doi.org/10.1134/S0022476617080248
3. A. G. Tskhovrebov, A. S. Novikov, and V. N. Khrustalev. Identification of supramolecular dimers in the crystal structure of (Z)-1-(((5-fluoropyridin-2-yl)amino)methylene)naphthalene-2(1H)-one via C(sp^2)–H···F hydrogen bonding: A combined experimental and theoretical study. *J*. *Struct*. *Chem*., **2021**, *62*(3), 460-466. https://doi.org/10.1134/S0022476621030136

4. S. Konar. Dicynamide bridged two new zig-zag 1-D Zn(II) coordination polymers of pyrimidine derived Schiff base ligands: Synthesis, crystal structures and fluorescence studies. *J. Mol. Struct*., **015**, *1092*, 34-43. https://doi.org/10.1016/j.molstruc.2015.02.048
5. T. Chen, Y. Xu, Z. Peng, A. Li, and J. Liu. Simultaneous enhancement of bioactivity and stability of laccase by Cu^{2+}/PAA/ PPEGA matrix for efficient biosensing and recyclable decontamination of pyrocatechol. *Anal. Chem*., **2017**, *89*, 2065-2072. https://doi.org/10.1021/acs.analchem.6b04691
6. M. Kurbanova, M. Ashfaq, M. N. Tahir, A. Maharramov, N. Dege, and A. Koroglu. Synthesis, crystal structure, supramolecular assembly exploration by Hirshfeld surface analysis and computational study of 6-bromo-2-oxo-2H-chromene-3-carbonitrile (BOOC). *J. Struct. Chem*., **2023**, *64*(2), 302-313. https://doi.org/10.1134/S0022476623020142
7. Z. Jabri, A. A. Thiruvalluvar, R. Sghyar, J. T. Mague, S. Sabir, Y. K. Rodi, E. H. Anouar, K. Misbahi, N. K. Sebbar, and E. M. Essassi. Synthesis, structure elucidation, Hirshfeld surface analysis, DFT, and molecular docking of new 6-bromo-imidazo[4,5-*b*]pyridine derivatives as potential tyrosyl-tRNA synthetase inhibitors. *J. Biomol. Struct. Dyn*., **2023**, 1-16. https://doi.org/10.1080/07391102.2023.2175258
8. S. Halder, A. Dey, J. Ortega-Castro, A. Frontera, P. P. Ray, and P. Roy. Irradiation specified conformational change in a small organic compound and its effect on electrical properties. *J. Phys. Chem. C*., **2016**, *120*, 25557-25563. https://doi.org/10.1021/acs.jpcc.6b10081
9. APEX-II, SAINT and SADABS. Madison, WI, USA: Bruker AXS Inc., **2008**.
10. G. M. Sheldrick. SHELXT - Integrated space-group and crystal-structure determination. *Acta Crystallogr*., *Sect. A: Found. Adv*., **2015**, *71*(1), 3-8. https://doi.org/10.1107/s2053273314026370
11. G. M. Sheldrick. Crystal structure refinement with SHELXL. *Acta Crystallogr*., *Sect. C: Cryst. Struct. Commun*., **2015**, *71*, 3-8. https://doi.org/10.1107/S2053229614024218
12. M. J. Frisch, G. W. Trucks, H. B. Schlegel, G. E. Scuseria, M. A. Robb, J. R. Cheeseman, G. Scalmani, V. Baone, G. A. Petersson, H. Nakatsuji, X. Li, M. Caricato, A. V. Marenich, J. Bloino, B. G. Janesko, R. Gomperts, B. Mennucci, H. P. Hratchian, J. V. Ortiz, A. F. Izmaylov, J. L. Sonnenberg, D. Williams-Young, F. Ding, F. Lipparini, F. Egidi, J. Goings, B. Peng, A. Petrone, T. Henderson, D. Ranasinghe, V. G. Zakrzewski, J. Gao, N. Rega, G. Zheng, W. Liang, M. Hada, M. Ehara, K. Toyota, R. Fukuda, J. Hasegawa, M. Ishida, T. Nakajima, Y. Honda, O. Kitao, H. Nakai, T. Vreven, K. Throssell, J. A. Montgomery Jr., J. E. Peralta, F. Ogliaro, M. J. Bearpark, J. J. Heyd, E. N. Brothers, K. N. Kudin, V. N. Staroverov, T. A. Keith, R. Kobayashi, J. Normand, K. Raghavachari, A. P. Rendell, J. C. Burant, S. S. Iyengar, J. Tomasi, M. Cossi, J. M. Millam, M. Klene, C. Adamo, R. Cammi, J. W. Ochterski, R. L. Martin, K. Morokuma, O. Farkas, J. B. Foresman, and D. J. Fox. Gaussian16, Revision C.01. Wallingford, CT, USA: Gaussian, Inc., **2016**.
13. M. A. Spackman and J. Dylan. Hirshfeld surface analysis, *CrystEngComm*, **2009**, *11*, 19-32. https://doi.org/10.1039/B818330A
14. M. J. Turner, J. J. McKinnon, S. K. Wolff, D. J. Grimwood, P. R. Spackman, D. Jayatilaka, and M. A. Spackman. CrystalExplorer17. Perth, Australia: University of Western Australia, **2017**.
15. H. A. Althobiti and S. A. Zabin. New Schiff bases of 2-(quinolin-8-yloxy) acetohydrazideand their Cu(II), and Zn(II) metal complexes: Their in vitro antimicrobial potentials and in silico physicochemical and pharmacokinetics properties. *Open Chem. J*., **2020**, *18*, 591-607. https://doi.org/10.1515/chem-2020-0085
16. H. M. Hassanin, R. A. T. Serya, W. R. Abd Elmoneam, and M. A. Mostafa. Synthesis and molecular docking studies of some novel Schiff bases incorporating 6-butylquinolinedione moiety as potential topoisomerase IIβ inhibitors. *R. Soc. Open Sci*., **2018**, *5*(6), 172407. https://doi.org/10.1098/rsos.172407
17. N. Boukabcha, A. Djafri, Y. Megrouss, O. Tamer, D. Avcı, M. Tuna, N. Dege, A. Chouaih, Y. Atalay, A. Djafri, and F. Hamzaoui. Synthesis, crystal structure, spectroscopic characterization and nonlinear optical properties of (Z)-N′-(2,4-dinitrobenzylidene)-2-(quinolin-8-yloxy) acetohydrazide. *J. Mol. Struct*., **2019**, *1194*, 112-123. https://doi.org/10.1016/j.molstruc.2019.05.074

18. S. G. Azimi, G. Bagherzade, M. R. Saberi, and Z. Amiri. Tehranizadeh, Discovery of new ligand with quinoline scaffold as potent allosteric inhibitor of HIV-1 and its copper complexes as a powerful catalyst for the synthesis of chiral benzimidazole derivatives, and in silico anti-HIV-1 studies. *Bioinorg*. *Chem*. *Appl*., **2023**, *2023*, 1-17. https://doi.org/10.1155/2023/2881582
19. A. A. El-Bindary, A. Z. El-Sonbati, M. A. Diab, N. A. El-Ghamaz, A. F. Shoair, and S. G. Nozha. Potentiometric studies and molecular docking of quinoline Schiff base and its metal complexes. *J. Mater*. *Environ*. *Sci*., **2016**, *7*(6), 1934-1947.
20. S. Halder, S. Dey, and P. Roy. A quinoline based Schiff-base compound as pH sensor. *RSC Adv*., **2015**, *5*, 54873-54881. https://doi.org/10.1039/C5RA07538F
21. R. Pucci and G. G. N. Angilella. Density functional theory, chemical reactivity, and the Fukui functions. *Found*. *Chem*., **2022**, *24*(1), 59-71. https://doi.org/10.1007/s10698-022-09416-z
22. R. Flores-Moreno, J. Melin, J. V. Ortiz, and G. Merino. Efficient evaluation of analytic Fukui functions. *J. Chem*. *Phys*., **2008**, *129*, 224105. https://doi.org/10.1063/1.3036926
23. M. Guin, S. Halder, S. Chatterjee, and S. Konar. Synthesis, X-ray crystal structure of Cu(II) 1D coordination Polymer: In view of Hirshfeld surface, FMO, molecular electrostatic potential (MEP) and natural bond orbital (NBO) analyses. *J. Mol*. *Struct*., **2022**, *1270*, 133949. https://doi.org/10.1016/j.molstruc.2022.133949
24. A. De, M. A. Kathait, P. Jain, and M. Guin. DFT investigation, Hirshfield analysis and molecular docking of Cu(II) complex of O-vanillin based ligand. *ChemistrySelect*, **2022**, *7*(42), e202202884. https://doi.org/10.1002/slct.202202884